ACS OMEGA

http://pubs.acs.org/journal/acsodf

Article

# High Performance of Carbon Monoxide Gas Sensor Based on a Novel PEDOT:PSS/PPA Nanocomposite

Mohammed O. Farea,* Hisham A. Alhadlaq, ZabnAllah M. Alaizeri, Abdullah A. A. Ahmed, Mohyeddine O. Sallam, and Maqusood Ahamed*

Cite This: *ACS Omega* 2022, 7, 22492−22499

Read Online

ACCESS | Metrics & More | Article Recommendations

**ABSTRACT:** In this work, the carbon monoxide (CO) detection property of poly(3,4-ethylenedioxythiophene)-poly(styrenesulfonate)/poly(*p*-anisidine) (PEDOT:PSS/PPA) nanocomposite was systematically investigated at room temperature. The PEDOT:PSS/PPA nanocomposite was synthesized by the cost-effective "in situ chemical oxidation polymerization" technique. The electric, optical, spectroscopic, and structural properties of the as-prepared nanomaterials were analyzed with *I*−*V*, UV−vis, Raman, Fourier transform infrared (FTIR), and X-ray diffraction (XRD) spectroscopies. Topological investigations of materials were conducted by atomic force microscopy (AFM). The gas-sensing performance of the PEDOT:PSS/PPA and PEDOT:PSS nanocomposites toward CO gas in the concentration range of 50−300 ppm at room temperature was explored, and their performances were compared. The PEDOT:PSS/PPA sensor shows a perfectly linear response to different concentrations (50−300 ppm) of CO gas ($R^2$ = 0.9885), and the response time and recovery time of the CO gas sensor (100 ppm) can be about 58 and 61 s, respectively, showing high sensitivity to CO gas and rapid response recovery with outstanding stability. Thus, the PEDOT:PSS/PPA-based sensors, with their impressive sensing performance, may give assurance for future high-performance CO-sensing applications.

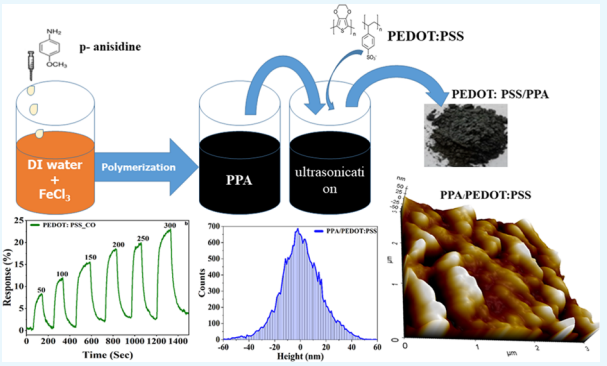


## 1. INTRODUCTION

With rapid surges in population and industrial development, concerns about environmental contamination have increased sharply to the top of the list of concerns. Currently, addressing the pollution problem is the top priority of scientists, environmentalists, and policymakers alike. Consequently, accurate screening and monitoring of contamination sources involving volatile organic compounds (VOCs),[1,2] heavy metal ions (HMI),[3] and poisonous gas species[4,5] have been the focus of researchers for the past few years due to their severe hazardous and toxic effects on the ecosystem and public health. Among the primary air pollutants, carbon monoxide (CO) is an odorless, colorless, flavorless, nonirritating, flammable, and hazardous gas pollutant that may be emanated into the atmosphere from natural sources or from the incomplete combustion of organic materials and fuels in the vehicle engines, industries, and coal-based power plants.[6] Exposure to high doses of CO for both short and long periods causes severe and persistent symptoms, like seizures, arrhythmias, loss of consciousness, and even death.[7] Indoor CO concentrations typically should not exceed 50 ppm over an 8 h cycle under normal conditions with good natural air exchange and ventilation.[8] Five thousand parts per million of CO is the lethal dose for humans after a 10 min exposure period.[9] For both human health and environmental safety, CO concentration must be accurately measured down to the permissible exposure limit (PEL) and up to levels that are instantly threatening to life.[10] Nowadays, developing low-cost, low-power, and room-temperature-operating gas sensors with good selectivity and sensitivity has drawn increased attention from researchers. Metal oxides (MOs) are the most commonly utilized and reported materials for detecting poisonous gases. Although MOs offer satisfactory sensitivity and good selectivity toward gases, these materials work at elevated temperatures, resulting in high power consumption; therefore, additional instrumentation arrangements are required.[11,12] Room-temperature (RT) operable gas sensors have achieved significant progress during the past few years. In this direction, conducting polymers have been extensively accepted as an

**Received:** March 21, 2022
**Accepted:** June 1, 2022
**Published:** June 21, 2022

alternative to MO semiconductor sensing materials to detect poisonous and hazardous gas species and VOCs.[13−15]

In this regard, organic conducting polymers (CPs) and their composites offer valuable properties such as tunable electrical/electronic characteristics, low energy intake, RT sensing ability, low cost of preparation, flexibility, prospects of tailoring their physical and chemical characteristics by exploiting different dopants, easy regulation of their morphology and shape, resistance to corrosion, fast response/recovery time, and comfort of deposition on diverse substrates.[16,17] Among the family of CPs, polythiophene (PTs) and its derivatives such as poly(3,4-ethylenedioxythiophene) (PEDOT), poly(3-hexylthiophene) (P3HT), and poly(3,4-ethylenedioxythiophene)-poly(styrenesulfonate) (PEDOT:PSS) are the most often used materials for chemeresistive gas singing owing to their easy fabrication, ultrahigh conductivity, and functionality at RT.[18−20] However, PEDOT:PSS suffers from poor solubility.[21] Moreover, environmental changes can affect its electrical properties significantly.[22] Solubility and stability shortcomings can be overcome by combining PEDOT:PSS with PPA. In the same direction, poly(*o*-anisidine)(POA) and poly(*p*-anisidine) (PPA) are the foremost derivatives of polyaniline (PANI). PPA with the methoxy ($O-CH_3$) group at the ortho site of the benzene is connected to the amino group. POA and PPA have excellent solution processability as they are soluble in organic solvents and acids.[23]

There have been several reports on the utilization of PEDOT:PSS in gas-sensing applications. For instance, Jang et al. have fabricated PEDOT nanorods by utilizing the reverse cylindrical-micelle-mediated interfacial polymerization method for HCl and $NH_3$ vapor detection. They found that the PEDOT sensor can respond to $NH_3$ and HCl concentrations down to 10 and 5 ppm, respectively.[24] Yang and his group reported reduced graphene oxide (RGO)/porous PEDOT nanocomposite prepared a room-temperature sensor by in situ polymerization method and LB deposition that is utilized for high-performance detection of $NO_2$ gas at the ppb level.[25] Sayyad et al. investigated the sensing behavior of PEDOT:PSS/graphene oxide (GO) composites prepared by solution processing method and employed as a chemiresistive-type SO2 gas sensor. They found that the prepared material displayed a brilliant response toward $SO_2$ in the range of 0.5−40 ppm with a fast response/recovery time of 81 and 92 s, respectively.[26] Our former results indicate that the composition of PEDOT:PSS and PPA by in situ chemical polymerization significantly improves the sensor performance. However, to the best of our knowledge, no effort has been devoted to synthesizing the PEDOT:PSS/PPA nanocomposite and utilizing it as a high-performance CO sensor. In light of this fact, we report the synthesis and use of PEDOT:PSS/PPA nanocomposite as a new, highly selective, highly sensitive, and cost-effective chemiresistive CO sensor.

Herein, we synthesized and developed a high-performance chemiresistive CO sensor based on the PEDOT:PSS/PPA nanocomposite prepared by the in situ chemical polymerization of the *p*-anisidine monomer in the presence of PEDOT:PSS. Copper-interdigitated electrodes (EDI) were used as sensor platforms. Pure PEDOT:PSS and PEDOT:PSS/PPA nanocomposites have been tested for their ability to detect CO at room temperature. The experimental findings show that the PEDOT:PSS/PPA sensor demonstrated excellent sensitivity, fast response/recovery times, very good selectivity, fair repeatability, and reversibility toward CO gas at room temperature.

## 2. EXPERIMENTAL SECTION

**2.1. Materials.** Poly(3,4-ethylenedioxythiophene)-polystyrenesulfonate (PEDOT:PSS), *p*-anisidine, sodium dodecyl sulfate (SDS), ferric chloride ($FeCl_3.6H_2O$), and ethanol were purchased from Thermo Fisher Scientific and used as received.

**2.2. Synthesis of Pure PAA and PEDOT:PSS/PPA Nanocomposite.** In situ polymerization of *p*-anisidine in an aqueous medium in the presence of PEDOT:PSS and an anionic surfactant, sodium dodecyl sulfate (SDS), was used to prepare the PEDOT:PSS/PPA nanocomposite. SDS (2.5 g) was dissolved in 150 mL of DDW and agitated for half an hour at room temperature. Then, 2.5 g of ferric chloride was added as an oxidant, and the mixture was rapidly stirred for another hour.[27] One hundred milliliters of the ready PEDOT:PSS aqueous solution was then poured into the above mixture. The mixture was then dispersed with 1 g of *p*-anisidine monomer and stirred continuously for 36 h at room temperature. The black PEDOT:PSS/PPA nanocomposite was washed with DDW and ethanol until its pH was neutralized. The solid substance was then dried in a vacuum oven at 50 °C overnight. A similar technique was used to prepare pure PPA by excluding the presence of PEDOT:PSS.

**2.3. Fabrication of Sensor Devices and Measurement Setup.** First, a few drops of the pure PEDOT:PSS and PEDOT:PSS/PPA nanocomposite was drop-cast onto the surface of the interdigitated copper electrode. Then, the deposited sensor devices were dried at 45 °C in an oven for around six hours. The gap between electrode fingers was bridged by a thin layer of PEDOT:PSS and PEDOT:PSS/PPA sensing materials. The sensor devices based on copper-interdigitated electrodes were then used as chemoresistive sensors and *I*−*V* measurements. The gas-sensing performance was performed using a dynamic gas-sensing setup having a 200 mL gas chamber and two mass flow controllers connected to the computer, as shown in Figure 1. The mass controller was

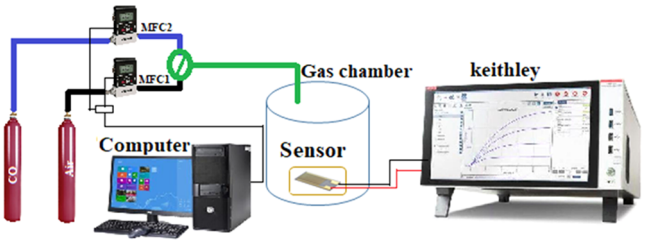


**Figure 1.** Schematic diagram of the dynamic gas system setup for CO gas sensing.

used to control and manage the desired concentration (50−300 ppm) of the CO gas. As shown in Figure 2, Keithley 2400 was used to record the current−voltage (*I*−*V*) characteristics and all sensing measurements of PEDOT:PSS and PEDOT:PSS/PPA at ambient temperature. The sensor's electrical resistance was measured using Keithley-4200 for the real-time monitoring of the resistance and current of the sensor when exposed to various concentrations of target gases. A dry airflow was used to keep the target gas concentration in check and ensure that the sensor's baseline was the same. The sensor response was defined as the difference in the resistivity of the


https://doi.org/10.1021/acsomega.2c01664
ACS Omega 2022, 7, 22492−22499

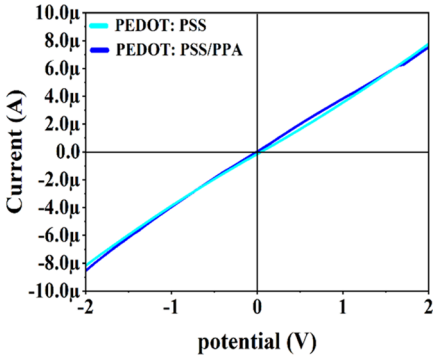


**Figure 2.** *I*–*V* characteristics of the PEDOT:PSS and PEDOT:PSS/PPA sensors.

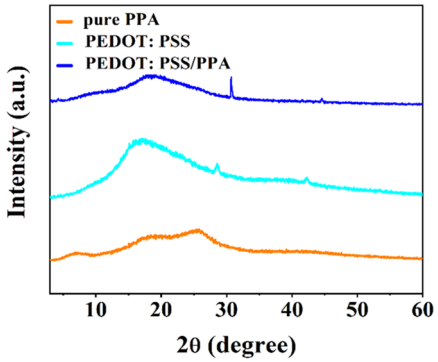


**Figure 3.** XRD patterns of PPA, PEDOT:PSS conducting polymer, and PEDOT:PSS/PPA nanocomposite.

sensor after and before exposure to the target gases, as shown in the following equation:

$$R = ((R_{air} - R_{gas})/R_{air}) \times (100\%) \quad (1)$$

The response time is the time for the sensor to reach 90% of its saturation resistance change after being exposed to targets. Recovery time is different because it describes how long it takes for a sensor to recover 10% of its initial resistance.

**2.4. Characterization.** The structural properties of the pristine PEDOT:PSS and PEDOT:PSS/PPA nanocomposite were investigated using a Diano XRD 800 diffractometer with Cu K radiation of the wavelength of 1.5406 nm and a Ni filter. The functional groups in the current PEDOT:PSS and PEDOT:PSS/PPA nanocomposite were detected using FTIR spectroscopy (Nicolet iS10) with a resolution of 4 $cm^{-1}$. A JASCO (V-570) spectrophotometer was used to conduct UV–vis spectroscopy of the sample in the range of 200–900 nm, the measurements were performed at room temperature and DDW was used as a solvent. A Keysight Technologies PICOPlus atomic force microscope (AFM) in the noncontact mode was used to obtain the surface morphology and surface roughness of the prepared samples. The Raman spectra of the synthesis materials were found with a Horiba Jobin Yvon spectrometer that used an argon laser with a wavelength of 514 nm to get them

## 3. RESULTS AND DISCUSSION

**3.1. XRD Analysis.** The microstructure of PPA, PEDOT:PSS, and PEDOT:PSS/PPA nanocomposite is inferred and characterized using X-ray diffraction (XRD). It can also be used to determine the degree of crystallinity. Figure 3 shows the X-ray patterns of virgin PPA, virgin PEDOT:PSS, and a nanocomposite of PEDOT:PSS/PPA. The XRD pattern of pure PPA reveals two broad characteristic peaks at $2\theta$ = 17.23 and 25.35°, which are caused by the scattering of the [001] plane of the poly(*p*-anisidine) matrix, indicating that PPA was successfully formed.[28] Because of its amorphous nature, PPA conducting polymer has broad peaks.[29] Figure 3 also shows the XRD patterns of the PEDOT:PSS film under examination. The interchain ring stacking inside the PEDOT:PSS matrix was responsible for the diffraction at around $2\theta$ = 16.90°.[30] The distances between the stacking [010] of the PEDOT:PSS chains are responsible for the sharp diffraction peaks at $2\theta$ = 28.45 and 42.25°.[31] The findings indicate that the XRD pattern matches that of pure PEDOT:PSS.

The X-ray diffraction of the PEDOT:PSS/PPA nanocomposite shows a hump or broad peak at around $2\theta$ = 18.54° resulting from an overlap between the $2\theta$ = 17.23° peak of PPA and the $2\theta$ = 16.90° peak of PEDOT:PSS. This overlapping indicates that the composite was successfully enhanced. It is noticeable that the intensity of the peak at $2\theta$ = 16.90° is decreased and shifted to 18.54° after the addition of PPA. Also, the diffraction peak at $2\theta$ = 28.45° is shifted to 30.88°, increasing its intensity. All of these changes confirm the interaction and complexation between PPA and PEDOT:PSS matrices.

**3.2. FTIR Measurement.** The nature of the interaction between PPA and the PEDOT:PSS matrices may be determined using FTIR measurements based on their vibration modes. Figure 4 depicts the FTIR spectra of pure PPA, pure

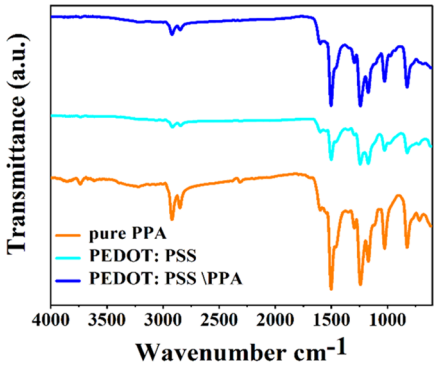


**Figure 4.** FTIR spectra of PPA, PEDOT:PSS conducting polymer, and PEDOT:PSS/PPA nanocomposite.

PEDOT:PSS, and PEDOT:PSS/PPA nanocomposite. In accordance with the literature review,[32] the transmittance bands of virgin PPA are found in the spectra at 3737, 2920, 1244, 1163, 1023, and 829 $cm^{-1}$. The quinoid ring units are responsible for the band at 1503 $cm^{-1}$. The PPA film generated by galvanostatic conditions was discovered to contain quinoid moieties. The transmittance bands at 2919 and 1498 $cm^{-1}$ in the FTIR spectra of PEDOT:PSS are attributed to the C–H stretching and C–O–H bending, respectively. A band of about 1239 $cm^{-1}$ may also be seen in the FTIR spectrum of the PEDOT:PSS film, which is created by asymmetric B–O stretching.[33] The C–O stretching vibration is responsible for the transmittance bands at 1068 and 1020 $cm^{-1}$. The observed transmittance bands at 840 $cm^{-1}$ were attributed to the C–H rocking. The FTIR spectra of the PEDOT:PSS/PPA nanocomposite shows all transmittance bands of the two pure polymers (at about 2920, 1503, 1244, 1177, 1034, and 816


https://doi.org/10.1021/acsomega.2c01664
ACS Omega 2022, 7, 22492–22499

$cm^{-1}$), which confirm the existence of PPA and PEDOT:PSS in the prepared film. The intensity changes for all previous bands when the two polymers are mixed. This change clarifies the interaction and complexation between PPA and PEDOT:PSS, as mentioned above in the XRD results.

**3.3. UV−vis Analysis.** Figure 5 shows the UV−vis spectra of PEDOT:PSS, PPA, and PEDOT:PSS/PPA nanocomposite

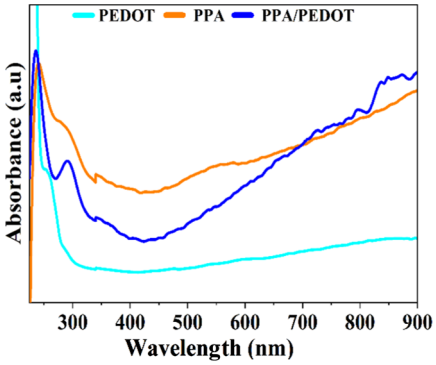


**Figure 5.** UV−vis spectra of PPA, PEDOT:PSS conducting polymer, and PEDOT:PSS/PPA nanocomposite.

in the absorption range of 190−900 nm. The absorption spectra of the PEDOT:PSS conducting polymer reveal a UV absorbance at 261 nm, which can be attributed to the phenyl groups substituted by PSS.[34] The broad bands between 500 and 700 nm might be assigned to the $\pi-\pi^*$ transitions of the thiophene ring. A free tail extending into the near-infrared region indicates the doped state of the PEDOT:PSS chains.[13,35] The PPA displays two characteristic absorption peaks, where a band at 285 nm and a broad absorption band between 470 and 580 nm appear, ascribed to the benzenoid $\pi-\pi^*$ transitions and quinoid rings,[28,36] respectively. The UV−vis spectra of the PEDOT:PSS/PPA nanocomposite exhibit the same absorption band at lower energy, inferring that the doping level of the nanocomposite is lower than that of homopolymers. As a result, the UV−vis absorption spectrum of PEDOT:PSS/PPA shows that adding PPA units to the PEDOT:PSS polymer chain may improve the doped state of the overall nanocomposite.

**3.4. Raman Analysis.** Raman spectroscopy is a powerful tool for studying the symmetric bond and is widely utilized to evaluate carbon materials and conducting polymers.[37] The Raman spectra of PEDOT:PSS, PPA, and PEDOT:PSS/PPA nanocomposite are shown in Figure 6. The high-intensity band at 1430 $cm^{-1}$ is ascribed to PEDOT and associated with the $C_\alpha = C_\beta$ symmetric stretching vibration. Compared to pure PEDOT:PSS, the shoulder bands between 1400 and 1500 $cm^{-1}$ become weaker. As seen in the PEDT:PSS spectrum, the bands located at 714, 982, and 1,256 $cm^{-1}$ are attributed to the symmetric C−S−C deformation, oxyethylene ring deformation, and $C_\alpha$-$C_\alpha$ inter-ring stretching, respectively.[38] PPA's Raman spectrum shows that the most intense bands at 1340 and 1560 $cm^{-1}$ are attributed to the bipolaronic N−H bending vibration and the C−N stretching vibration of the cation radical species.[39] Furthermore, the Raman spectra of the PEDOT-PSS/PPA nanocomposites have a shape that contains all peaks and is almost identical to that of PPA, with a minor change in the peak location from 1340 to 1609 $cm^{-1}$, indicating that the PEDOT:PSS/PPA nanocomposites are successfully synthesized.

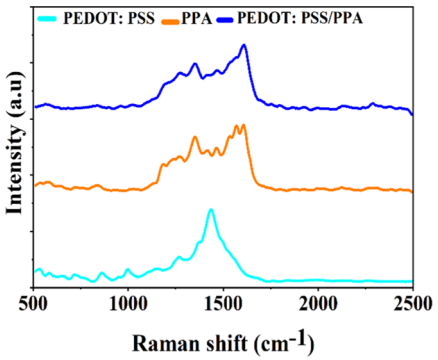


**Figure 6.** Raman spectra of PPA, PEDOT:PSS conducting polymer, and PEDOT:PSS/PPA nanocomposite.

**3.5. Morphology Analysis.** The effect of the PPA matrix on the morphology of the PEDOT:PSS latex is investigated using AFM, as revealed in Figure 7. These figures present a three-dimensional (3D) AFM topographical portrait in an area of 3 $\mu$m × 3 $\mu$m of pure PPA, PEDOT:PSS, and PEDOT:PSS/PPA thin films deposited by the drop-casting method. In Figure 7a, the pristine PEDOT:PSS exhibits a relatively smooth surface, representing a few defects. In Figure 7c, the surface morphology of the pure PPA matrix demonstrates the aggregating nature of particles in several valleys and voids, indicating that the high surface area of PPA matched that of the PEDOT:PSS. The inclusion of the PEDOT:PSS latex in the PPA matrix in the PEDOT:PSS/PPA nanocomposite results in an even and regulated distribution of particles, with the occurrence of a variety of nanoflanges and polygonals of distinct dimensions, as is clear from Figure 7e. Histograms of the particle's height distributions of all of the pure materials and the composite are shown in Figure 7b,d,f. All materials exhibit a nearly Gaussian symmetrical height. However, the height distribution ranges vary from one material to another, reflecting their surface area and surface roughness, as clearly indicated in Table 1. After incorporating PPA into PEDOT:PSS, the roughness and surface area of the sensing material increased dramatically, resulting in a larger roughness of the sensing material with more active sites available, making it desirable for gas-sensing applications.[13]

**3.6. Gas Sensor Analysis.** For this study, a PEDOT:PSS/PPA sensor was made, and its gas-sensing capabilities toward CO gas were investigated at ambient temperature. The study found that mixing PEDOT:PSS with PPA made PEDOT:PSS more sensitive and enhanced its sensing performance. Figure 8a shows the PEDOT:PSS/PPA nanocomposite response curves when exposed to varied CO concentrations. As a reference point, the same experimental circumstances were used to fabricate and test a sensor based on pure PEDOT:PSS, as shown in Figure 8b. PEDOT:PSS has CO-sensing capabilities at ambient temperature, unlike metal oxide semiconductor materials that can work at high temperatures. Although PEDOT:PSS has high conductivity properties, it is insoluble in the solution, has small surface roughness, and has a low surface area, as shown by AFM results. Therefore, the observed enhancement in the sensitivity of the PEDOT:PSS/PPA nanocomposite can be attributed to the presence of PPA, which has a high surface area and high surface roughness. When the sensors were exposed to CO gas, the resistance of both sensors increased and reverted to practically the starting value when the gas was removed and the sensors were exposed


https://doi.org/10.1021/acsomega.2c01664
ACS Omega 2022, 7, 22492−22499

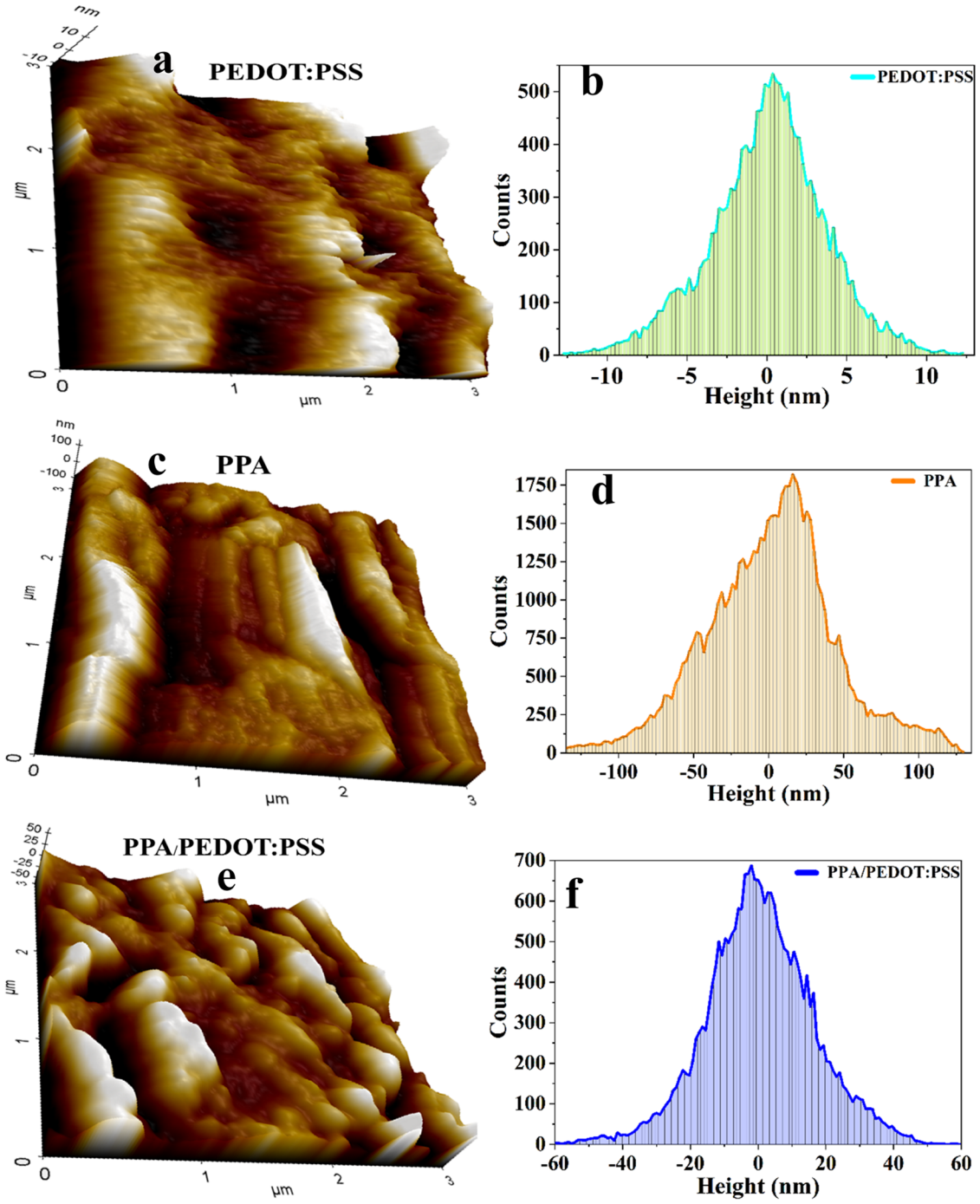


**Figure 7.** AFM topographical 3D images and histogram of the height distribution of PPA, PEDOT:PSS, and PPA/PEDOT:PSS.

**Table 1. Surface Area and Roughness of the Materials**

| sr. no | material | surface area ($\mu m^2$) | surface roughness (nm) |
|---|---|---|---|
| 1 | PPA | 9.9927 | 33.970 |
| 2 | PEDOT:PSS | 9.0071 | 29.843 |
| 3 | PPA/PEDOT:PSS | 9.2481 | 115.384 |

to dry air. When CO molecules interacted with sensing materials, more electrons were transferred to their surfaces and equipped most of the holes, resulting in a decrease in free electrons and an increase in the resistance of the sensing materials; as seen from the figure, the resistance of sensor increased with the increase in the gas concentration.[40] In our work, the sensor was investigated in a wide CO concentration range (50−300 ppm) with a lower dedication limit of 50 ppm, which was the permitted level of exposure to CO gas according to the Occupational Safety and Health Administration (OSHA). Compared to a pure PEDOT:PSS-based sensor, the PEDOT:PSS/PPA-based sensor had a 32% higher response. A linear regression equation was obtained for PEDOT:PSS as $y = 9.33 + 0.08x$, where $x$ is the CO gas concentration in ppm and $y$ is the gas response, with a correlation coefficient ($R^2$) of 0.9885, suggesting a solid linear association between the response and the CO concentration as shown in Figure 9a. In addition, our sensor exhibited a fast response and quick recovery time, as shown in Figure 9b. The


https://doi.org/10.1021/acsomega.2c01664
ACS Omega 2022, 7, 22492−22499

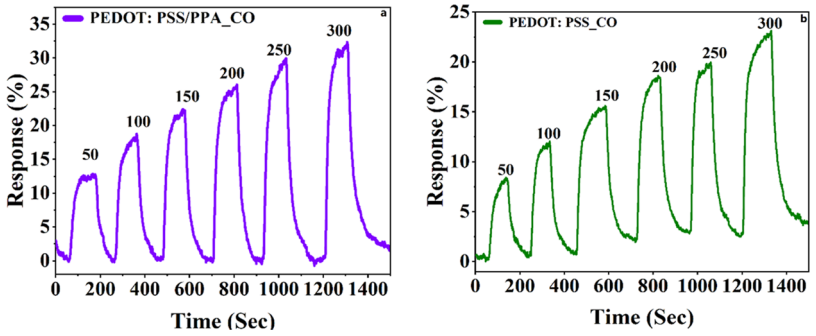


**Figure 8.** Real-time responses of (a) PEDOT:PSS/PPA nanocomposite and (b) pure PEDOT:PSS sensor toward different concentrations of CO gas.

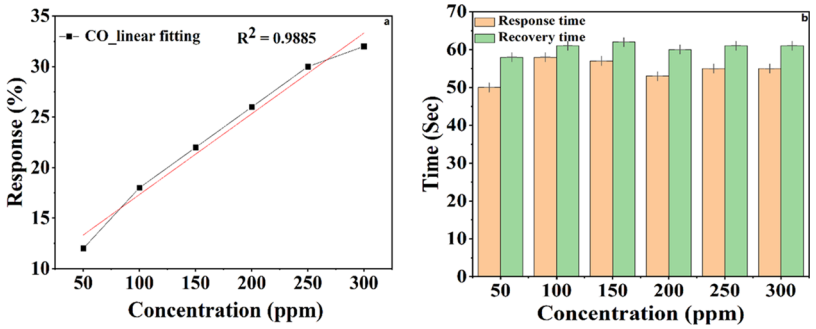


**Figure 9.** (a) Linear regression of sensor response as function with CO concentration (b) response and recovery time at all concentrations of CO.

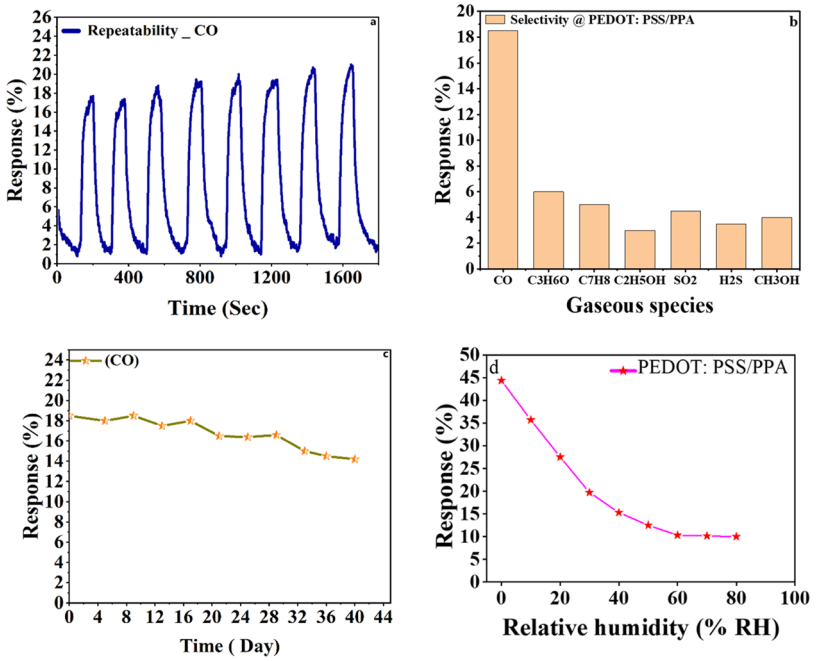


**Figure 10.** Sensing performance of the PEDOT:PSS/PPA sensor at 100 ppm of CO. (a) Repeatability, (b) selectivity, and (c) stability toward different interference gases, and (d) humidity effect on the PEDOT:PSS/PPA sensor.

response and recovery times of the PEDOT:PSS/PPA sensor toward all CO concentrations are calculated to be 50 s/58 s, 58 s/61 s, 57 s/62 s, 53 s/60 s, 55 s/61 s, and 55 s/61 s, respectively. The PEDOT:PSS/PPA-based sensor was subjected to eight consecutive pulses of CO gas to test its reliability. The sensor maintained the same levels for eight cycles of CO gas exposure, as shown in Figure 10a. There was minimal difference in the sensor's continuous response to different concentrations of CO. The results showed that the CO gas sensor was highly reversible and reproducible after repeated exposure and removal of CO gas molecules. Sophisticated gas sensors must be able to distinguish between different types of gases. Therefore, the selectivity of the sensor was a critical criterion for its practical application. Figure 10b depicts the response of the PEDOT:PSS/PPA sensor toward 100 ppm of various gases (carbon monoxide, acetone, toluene,


https://doi.org/10.1021/acsomega.2c01664
ACS Omega 2022, 7, 22492−22499

ethanol, and methanol) measured at room temperature. The response of the PEDOT:PSS/PPA sensor to 100 ppm carbon monoxide, acetone, toluene, ethanol, sulfur dioxide, hydrogen sulfide, and methanol was only 18.5, 6, 5, 3, 4.5, 3.5, and 4%, respectively, demonstrating that the PEDOT:PSS/PPA nanocomposite had high selectivity toward CO and low cross-sensitivity to other gases. Long-term stability is the pivotal standard for the practical application of gas sensors. At room temperature, the long-term stability of the PEDOT:PSS sensor was determined by evaluating its responses to 100 ppm CO every four days over a period of 44 days, as shown in Figure 10c. According to the above result, there was only a small decrease in responsiveness over the course of 44 days. It was envisaged that humidity influenced the functioning of the PEDOT:PSS/PPA sensor. Consequently, at room temperature, the impact of humidity on the behavior of the PEDOT:PSS/PPA sensor was investigated. Figure 10c depicts the connection between the responses of the PEDOT:PSS/PPA sensor and relative humidity from 0 to 80% throughout the range of temperatures. According to the results of the humidity test, the response of the PEDOT:PSS/PPA sensor was reduced when the relative humidity was increased. Although the response dropped linearly from 10 to 40% RH, a little amount of saturation was found after 60% RH, with a modest decrease in response at up to 80% RH, which corresponded to the reported result. The effect of humidity proved the adsorption of water molecules. Therefore, moisture had a significant impact on the performance of the PEDOT:PSS/PPA sensor.

## 4. CONCLUSIONS

In the current work, an efficient, reversible, and reliable carbon monoxide sensor based on the PEDOT:PSS and PEDOT:PSS/PPA nanocomposite was successfully fabricated. An in situ polymerization technique was used to prepare a novel PEDOT:PSS/PPA compound effective for CO sensing. The structural, spectroscopic, and morphological features of the as-prepared sensing materials were studied utilizing XRD, FTIR, UV−vis, Raman spectroscopy, and AFM. The gas-sensing characteristics of the developed sensors were evaluated at room temperature for different CO concentrations.

## AUTHOR INFORMATION


### Corresponding Authors

**Mohammed O. Farea** − *Department of Physics, Faculty of Science, Mansoura University, Mansoura 35516, Egypt;* orcid.org/0000-0001-5414-9706; Email: mhd.omar1984@gmail.com

**Maqusood Ahamed** − *Department of Physics and Astronomy, College of Science, King Saud University, Riyadh 11451, Saudi Arabia;* orcid.org/0000-0001-6025-1950; Email: mahamed@ksu.edu.sa

### Authors

**Hisham A. Alhadlaq** − *Department of Physics and Astronomy, College of Science, King Saud University, Riyadh 11451, Saudi Arabia;* orcid.org/0000-0002-3073-7025

**ZabnAllah M. Alaizeri** − *Department of Physics and Astronomy, College of Science, King Saud University, Riyadh 11451, Saudi Arabia*

**Abdullah A. A. Ahmed** − *Center for Hybrid Nanostructures (CHyN) and Physics Department, University Hamburg, 20146 Hamburg, Germany*

**Mohyeddine O. Sallam** − *Department of Physics, University of Mysore, Mysuru 570006, India*

Complete contact information is available at: https://pubs.acs.org/10.1021/acsomega.2c01664


### Notes

The authors declare no competing financial interest.

The data that support the findings of this study are available on request from the corresponding author. The data are not publicly available because it is part of unpublished data for another study.

## ACKNOWLEDGMENTS

The authors extend their sincere appreciation to researchers supporting project number (RSP-2021/129), King Saud University, Riyadh, Saudi Arabia for funding this research.

## REFERENCES


(1) Mohammed, H. Y.; Farea, M. A.; Ingle, N. N.; Sayyad, P. W.; Al-Gahouari, T.; Mahadik, M. M.; Bodkhe, G. A.; Shirsat, S. M.; Shirsat, M. D. Review—Electrochemical Hydrazine Sensors Based on Graphene Supported Metal/Metal Oxide Nanomaterials. *J. Electrochem. Soc.* **2021**, *168*, No. 106509.

(2) Rao, D.; Sheng, Q.; Zheng, J. Preparation of Flower-like Pt Nanoparticles Decorated Chitosan-Grafted Graphene Oxide and Its Electrocatalysis of Hydrazine. *Sensors Actuators, B* **2016**, *236*, 192−200.

(3) Lu, M.; Deng, Y.; Luo, Y.; Lv, J.; Li, T.; Xu, J.; Chen, S. W.; Wang, J. Graphene Aerogel-Metal-Organic Framework-Based Electrochemical Method for Simultaneous Detection of Multiple Heavy-Metal Ions. *Anal. Chem.* **2019**, *91*, 888−895.

(4) Roy, A.; Ray, A.; Sadhukhan, P.; Naskar, K.; Lal, G.; Bhar, R.; Sinha, C.; Das, S. Polyaniline-Multiwalled Carbon Nanotube (PANI-MWCNT): Room Temperature Resistive Carbon Monoxide (CO) Sensor. *Synth. Met.* **2018**, *245*, 182−189.

(5) Wanna, Y.; Srisukhumbowornchai, N.; Tuantranont, A.; Wisitsoraat, A.; Thavarungkul, N.; Singjai, P. The Effect of Carbon Nanotube Dispersion on CO Gas Sensing Characteristics of Polyaniline Gas Sensor. *J. Nanosci. Nanotechnol.* **2006**, *6*, 3893−3896.

(6) Farea, M. A.; Mohammed, H. Y.; Shirsat, S. M.; Sayyad, P. W.; Ingle, N. N.; Al-Gahouari, T.; Mahadik, M. M.; Bodkhe, G. A.; Shirsat, M. D. Hazardous Gases Sensors Based on Conducting Polymer Composites: Review. *Chem. Phys. Lett.* **2021**, *776*, No. 138703.

(7) Weaver, L. K. Carbon Monoxide Poisoning. *Crit. Care Clin.* **1999**, *15*, 297−317.

(8) EPA. Carbon Monoxide's Impact on Indoor Air Quality _ Indoor Air Quality (IAQ) _ US EPA. https://www.epa.gov/indoor-air-quality-iaq/carbon-monoxides-impact-indoor-air-quality (accessed February 16, 2022).

(9) Mirzaei, A.; Park, S.; Sun, G. J.; Kheel, H.; Lee, C. CO Gas Sensing Properties of In4Sn3O12 and TeO2 Composite Nanoparticle Sensors. *J. Hazard. Mater.* **2016**, *305*, 130−138.

(10) Sen, T.; Shimpi, N. G.; Mishra, S.; Room Temperature, C. O. Room temperature CO Sensing by Polyaniline/Co3O4 Nanocomposite. *J. Appl. Polym. Sci.* **2016**, *133*, No. 42.

(11) Kumar, A.; Sanger, A.; Kumar, A.; Chandra, R. Highly Sensitive and Selective CO Gas Sensor Based on a Hydrophobic SnO2/CuO Bilayer. *RSC Adv.* **2016**, *6*, 47178−47184.

(12) Yin, X. T.; Guo, X. M. Selectivity and Sensitivity of Pd-Loaded and Fe-Doped SnO2 Sensor for CO Detection. *Sensors Actuators, B* **2014**, *200*, 213−218.

(13) Mohammed, H. Y.; Farea, M. A.; Sayyad, P. W.; Ingle, N. N.; Al-Gahouari, T.; Mahadik, M. M.; Bodkhe, G. A.; Shirsat, S. M.; Shirsat, M. D. Selective and Sensitive Chemiresistive Sensors Based on Polyaniline/Graphene Oxide Nanocomposite: A Cost-Effective Approach. *J. Sci. Adv. Mater. Devices* **2022**, *7*, No. 100391.




https://doi.org/10.1021/acsomega.2c01664
*ACS Omega* 2022, 7, 22492−22499

(14) Nasresfahani, S.; Zargarpour, Z.; Sheikhi, M. H.; Nami Ana, S. F. Improvement of the Carbon Monoxide Gas Sensing Properties of Polyaniline in the Presence of Gold Nanoparticles at Room Temperature. *Synth. Met.* **2020**, *265*, No. 116404.
(15) Pandey, S. Highly Sensitive and Selective Chemiresistor Gas/Vapor Sensors Based on Polyaniline Nanocomposite: A Comprehensive Review. *J. Sci.: Adv. Mater. Devices* **2016**, *1*, 431−453.
(16) Janata, J.; Josowicz, M. Conducting Polymers in Electronic Chemical Sensors. *Nat. Mater.* **2003**, *2*, 19−24.
(17) Park, S. J.; Park, C. S.; Yoon, H. Chemo-Electrical Gas Sensors Based on Conducting Polymer Hybrids. *Polymers* **2017**, *9*, No. 155.
(18) Pasha, A.; Khasim, S.; Al-Hartomy, O. A.; Lakshmi, M.; Manjunatha, K. G. Highly Sensitive Ethylene Glycol-Doped PEDOT−PSS Organic Thin Films for LPG Sensing. *RSC Adv.* **2018**, *8*, 18074−18083.
(19) Zhao, Q.; Jamal, R.; Zhang, L.; Wang, M.; Abdiryim, T. The Structure and Properties of PEDOT Synthesized by Template-Free Solution Method. *Nanoscale Res. Lett.* **2014**, *9*, No. 557.
(20) Cheon, H. J.; Shin, S. Y.; Tran, V. Van.; Park, B.; Yoon, H.; Chang, M. Preparation of Conjugated Polymer/Reduced Graphene Oxide Nanocomposites for High-Performance Volatile Organic Compound Sensors. *Chem. Eng. J.* **2021**, *425*, No. 131424.
(21) Schultheiss, A.; Gueye, M.; Carella, A.; Benayad, A.; Pouget, S.; Faure-Vincent, J.; Demadrille, R.; Revaux, A.; Simonato, J. P. Insight into the Degradation Mechanisms of Highly Conductive Poly(3,4-Ethylenedioxythiophene) Thin Films. *ACS Appl. Polym. Mater.* **2020**, *2*, 2686−2695.
(22) Nardes, A. M.; Kemerink, M.; de Kok, M. M.; Vinken, E.; Maturova, K.; Janssen, R. A. J. Conductivity, Work Function, and Environmental Stability of PEDOT:PSS Thin Films Treated with Sorbitol. *Org. Electron.* **2008**, *9*, 727−734.
(23) Mahajan, L. H.; Mhaske, S. T. Composite Microspheres of Poly(o-Anisidine)/TiO2. *Mater. Lett.* **2012**, *68*, 183−186.
(24) Jang, J.; Chang, M.; Yoon, H. Chemical Sensors Based on Highly Conductive Poly(3,4-Ethylene- Dioxythiophene) Nanorods. *Adv. Mater.* **2005**, *17*, 1616−1620.
(25) Yang, Y.; Li, S.; Yang, W.; Yuan, W.; Xu, J.; Jiang, Y. In Situ Polymerization Deposition of Porous Conducting Polymer on Reduced Graphene Oxide for Gas Sensor. *ACS Appl. Mater. Interfaces* **2014**, *6*, 13807−13814.
(26) Memarzadeh, R.; Noh, H. B.; Javadpour, S.; Panahi, F.; Feizpour, A.; Shim, Y. B. Carbon Monoxide Sensor Based on a B2HDDT-Doped PEDOT:PSS Layer. *Bull. Korean Chem. Soc.* **2013**, *34*, 2291−2296.
(27) Hu, C.; Li, Y.; Zhang, N.; Ding, Y. Synthesis and Characterization of a Poly(o-Anisidine)-SiC Composite and Its Application for Corrosion Protection of Steel. *RSC Adv.* **2017**, *7*, 11732−11742.
(28) Boutaleb, N.; Chouli, F.; Benyoucef, A.; Zeggai, F. Z.; Bachari, K. A Comparative Study on Surfactant Cetyltrimethylammonium-bromide Modified Clay-Based Poly(p-Anisidine) Nanocomposites: Synthesis, Characterization, Optical and Electrochemical Properties. *Polym. Compos.* **2021**, *42*, 1648−1658.
(29) K, R.; Velmani, N.; Tamilselvi, D. Electrical Conductivity Study of Poly(p-Anisidine) Doped and Undoped ZnO Nanocomposite. *Mediterr. J. Chem.* **2019**, *9*, 403−410.
(30) Abd-Elghany, R.; Khoder, H.; Khalil, R.; El-Mansy, M. Study on Nonlinear Conduction of PEDOT:PSS Conducting Polymer. *Benha J. Appl. Sci.* **2021**, *6*, 47−56.
(31) Zhou, J.; Anjum, D. H.; Chen, L.; Xu, X.; Ventura, I. A.; Jiang, L.; Lubineau, G. The Temperature-Dependent Microstructure of PEDOT/PSS Films: Insights from Morphological, Mechanical and Electrical Analyses. *J. Mater. Chem. C* **2014**, *2*, 9903−9910.
(32) Radja, I.; Djelad, H.; Morallon, E.; Benyoucef, A. Characterization and Electrochemical Properties of Conducting Nanocomposites Synthesized from P-Anisidine and Aniline with Titanium Carbide by Chemical Oxidative Method. *Synth. Met.* **2015**, *202*, 25−32.
(33) Yagci, Ö.; Yesilkaya, S. S.; Yüksel, S. A.; Ongül, F.; Varal, N. M.; Kus, M.; Günes, S.; Icelli, O. Effect of Boric Acid Doped PEDOT:PSS Layer on the Performance of P3HT:PCBM Based Organic Solar Cells. *Synth. Met.* **2016**, *212*, 12−18.
(34) Sun, D. C.; Sun, D. S. The Synthesis and Characterization of Electrical and Magnetic Nanocomposite: PEDOT/PSS−Fe3O4. *Mater. Chem. Phys.* **2009**, *118*, 288−292.
(35) Wei, Z.; Wan, M.; Lin, T.; Dai, L. Polyaniline Nanotubes Doped with Sulfonated Carbon Nanotubes Made via a Self-Assembly Process. *Adv. Mater.* **2003**, *15*, 136−139.
(36) Hammadi, F. Z.; Belardja, M. S.; Lafjah, M.; Benyoucef, A. Studies of Influence of ZrO2 Nanoparticles on Reinforced Conducting Polymer and Their Optical, Thermal and Electrochemical Properties. *J. Inorg. Organomet. Polym. Mater.* **2021**, *31*, 1176−1184.
(37) Chiu, W. W.; Travaš-Sejdić, J.; Cooney, R. P.; Bowmaker, G. A. Studies of Dopant Effects in Poly(3,4-Ethylenedioxythiophene) Using Raman Spectroscopy. *J. Raman Spectrosc.* **2006**, *37*, 1354−1361.
(38) Tamburri, E.; Orlanducci, S.; Toschi, F.; Terranova, M. L.; Passeri, D. Growth Mechanisms, Morphology, and Electroactivity of PEDOT Layers Produced by Electrochemical Routes in Aqueous Medium. *Synth. Met.* **2009**, *159*, 406−414.
(39) Synthesis and characterization of novel poly(o-anisidine)... - Google Scholar.
(40) Arabloo, F.; Javadpour, S.; Memarzadeh, R.; Panahi, F.; Davazdah Emami, M.; Shariat, M. H. The Interaction of Carbon Monoxide to Fe(III)(Salen)-PEDOT:PSS Composite as a Gas Sensor. *Synth. Met.* **2015**, *209*, 192−199.


https://doi.org/10.1021/acsomega.2c01664
*ACS Omega* 2022, 7, 22492−22499